


Chiral-Flux-Phase-Based Topological Superconductivity in Kagome Systems with Mixed Edge Chiralities

Junjie Zeng¹, Qingming Li², Xun Yang¹, Dong-Hui Xu^{1,*}, and Rui Wang^{1,3,†}

¹*Institute for Structure and Function and Department of Physics and Chongqing Key Laboratory for Strongly Coupled Physics, Chongqing University, Chongqing 400044, People's Republic of China*

²*Department of Physics, Shijiazhuang University, Shijiazhuang, Hebei 050035, People's Republic of China*

³*Center of Quantum materials and devices, Chongqing University, Chongqing 400044, People's Republic of China*

 (Received 30 March 2023; revised 25 June 2023; accepted 4 August 2023; published 25 August 2023)

Recent studies have attracted intense attention on the quasi-2D kagome superconductors AV_3Sb_5 ($A = K, Rb, \text{ and } Cs$) where the unexpected chiral flux phase (CFP) associates with the spontaneous time-reversal symmetry breaking in charge density wave states. Here, commencing from the 2-by-2 charge density wave phases, we bridge the gap between topological superconductivity and time-reversal asymmetric CFP in kagome systems. Several chiral topological superconductor (TSC) states featuring distinct Chern numbers emerge for an s -wave or a d -wave superconducting pairing symmetry. Importantly, these CFP-based TSC phases possess unique gapless edge modes with mixed chiralities (i.e., both positive and negative chiralities), but with the net chiralities consistent with the Bogoliubov–de Gennes Chern numbers. We further study the transport properties of a two-terminal junction, using Chern insulator or normal metal leads via atomic Green's function method with Landauer–Büttiker formalism. In both cases, the normal electron tunneling and the crossed Andreev reflection oscillate as the chemical potential changes, but together contribute to plateau transmissions (1 and $\frac{3}{2}$, respectively) that exhibit robustness against disorder. These behaviors can be regarded as the signature of a TSC hosting edge states with mixed chiralities.

DOI: [10.1103/PhysRevLett.131.086601](https://doi.org/10.1103/PhysRevLett.131.086601)

Introduction.—Dissipationless transport is long longed for by scientific community. Its early realization is brought up by the advent of superconductivity [1,2]. In a superconductor, electrons pair to form Cooper pairs, undergoing condensation below the critical temperature, which carry a nondissipative supercurrent. Another possibility is provided by a more recent achievement on the states of matter with nontrivial topology. Typical examples are the quantum Hall state [3–5] and the quantum anomalous Hall state [6–8]. They exhibit vanishing longitudinal resistivity and are quite robust because of their nature in topology [9]. Then what if a conventional superconductor and the quantum Hall state are combined? The answer could be time-reversal symmetry breaking chiral topological superconductivity [10]. Chiral topological superconductors (TSCs) accommodate Majorana zero modes [11–16], which are attractive building blocks for quantum computers [17–20], when creating superconducting vortices. As naturally occurring chiral TSCs are rare, it is important to engineer chiral TSCs in artificial structures, where an external magnetic field or magnetization is usually considered a necessary ingredient to break time-reversal symmetry [10,21,22].

Very recently, the quasi-two-dimensional (2D) AV_3Sb_5 ($A = K, Rb, \text{ and } Cs$) family of materials has been experimentally confirmed as a platform for various exotic quantum phenomena, including nontrivial band topology [23,24],

unconventional charge density wave (CDW) ordered states such as the 2-by-2 vector charge density wave (vCDW), the charge bond order (CBO), and the time-reversal symmetry breaking chiral flux phase (CFP) [24–27], superconductivity [23,28–34], as well as their coexistence [35,36]. Moreover, although the materials themselves take three-dimensional structures, those important features are believed to originate from their 2D kagome lattice substructure [37–42].

Specifically, in that family of materials, the superconducting pairing symmetry is at first supported as conventional s wave [43–46], but experimental evidence of unconventional pairing soon follows up, as the absence of the Hebel-Slichter resonant peak under pressure [35] together with the V-shaped dI/dV curves from the scanning tunneling microscopy measurement [47,48]. Additionally, inside superconducting vortices, a robust and nonsplit zero-bias conductance peak has been observed, indicating the possible presence of Majorana bound states [47]. While relevant advancements are indeed very encouraging, it has been largely unexplored whether the coupling between superconductivity and time-reversal symmetry breaking CFP induces novel nontrivial phenomena. To be specific, there have been so far at least three unclear issues about this family of materials: Issue (I) the undetermined superconductivity pairing symmetry; Issue

(II) the connection between topological superconductivity and time-reversal asymmetric CFP; and Issue (III) the basic transport characteristics of corresponding gapless edge states, if Issue (II) is established.

Motivated by the above issues, in this Letter, we study the interplay between superconductivity and charge orders in a Rashba spin-orbit coupled kagome lattice by considering three possible CDW orderings and two spin-singlet (s and $d_{x^2-y^2}$ wave) pairing symmetries. We find that starting from the time-reversal symmetry breaking CFP state, chiral TSC phases emerge for both singlet pairings, but with distinct phase diagrams and different scenarios for chiralities of the gapless edge modes. Because of the status of mixing chiralities, we focus on a two-terminal device with two typical leads, such as Chern insulator and metal leads, and the tunneling signals plateaus at distinct values 1 and $\frac{3}{2}$, respectively, for the s -wave-based TSC with $\mathcal{N} = 1$. Moreover, we also investigate the transport property in the presence of disorder, and the results show that the quantized plateaus are robust. After clarifying all above, we then naturally provide clues to the first issue in distinguishing between pairing symmetries. Because in the situations we have considered, there are no common TSC Chern numbers between the s -wave and the $d_{x^2-y^2}$ -wave cases.

Model Hamiltonian.—To achieve the purpose stated above, we build a Bogoliubov–de Gennes (BdG) model based on the 2-by-2 CDW tight-binding Hamiltonian [24,25] with ingredients including Rashba spin-orbit coupling (RSOC) due to the breaking of inversion symmetry by the substrate and two kinds of superconducting pairing terms: the conventional s wave and the unconventional $d_{x^2-y^2}$ wave. In the second quantization form, it can be written as

$$\begin{aligned}
 H_{\text{BdG}} &= H_0 + H_{\text{CDW}} + H_{\text{RSOC}} + H_{\text{SC}}, \\
 H_0 &= \sum_i c_i^\dagger (-\mu) c_i + \sum_{\langle ij \rangle} c_i^\dagger (-t) c_j, \\
 H_{\text{CDW}} &= \sum_i c_i^\dagger (-\lambda_i^{\text{vCDW}}) c_i + \sum_{\langle ij \rangle} c_i^\dagger (-\lambda_{ij}^{\text{CBO}} - i\lambda_{ij}^{\text{CFP}}) c_j, \\
 H_{\text{RSOC}} &= i\alpha \sum_{\langle ij \rangle} c_i^\dagger (\mathbf{s} \times \hat{\mathbf{d}}_{ij})_z c_j, \\
 H_{\text{SC}} &= \sum_i c_{i\uparrow}^\dagger \Delta^s c_{i\downarrow}^\dagger + \sum_{\langle ij \rangle} c_{i\uparrow}^\dagger \Delta_{ij}^{d_{x^2-y^2}} c_{j\downarrow}^\dagger + \text{H.c.}, \quad (1)
 \end{aligned}$$

where $c_i^\dagger = (c_{i\uparrow}^\dagger, c_{i\downarrow}^\dagger)$ is the electron creation operator at the site i with the spin degree of freedom included. The pristine term H_0 contains the chemical potential μ and the nearest hopping $t = 1$, which we choose to be the energy unit hereafter. The second term H_{CDW} describes the three kinds of CDW states, among which we consider only one at a time and they can be quantitatively mapped to graphs, respectively, into panels (a)–(c) of Fig. 1. The bracket $\langle \dots \rangle$ under the summation symbol means the first nearest neighbors. The third term H_{RSOC} is the RSOC measured by the parameter α

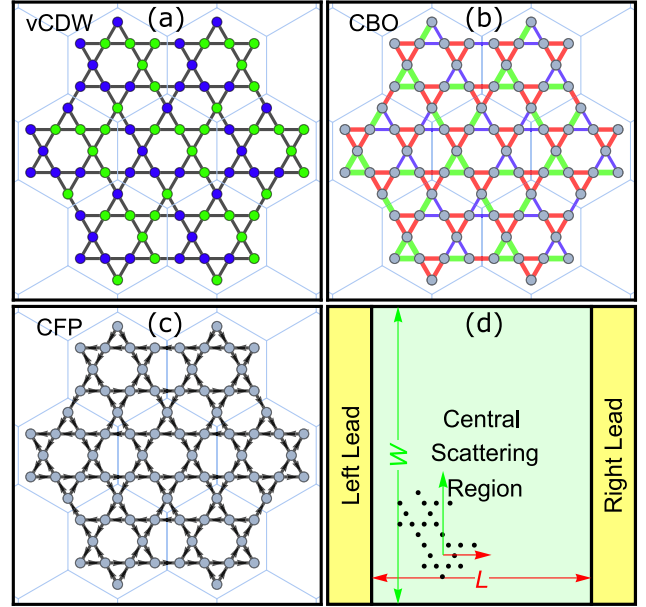


FIG. 1. Panels (a)–(c): Graph representations of the three kinds of CDW states, where the light-blue-edged hexagons represent the primitive cells. In panel (a), the blue and green nodes have negative and positive on-site energy modification to the chemical potential $-(\mu \pm \lambda^{\text{vCDW}})$, and the black edge connecting a pair of nodes represents the nearest-neighbor hopping. In panel (b), all the on-site energies are the same, but the hoppings are modified: the red edges stands for the normal hopping $-t$, the thicker green ones enhanced $-(t + \lambda^{\text{CBO}})$, and the thinner blue ones weakened $-(t - \lambda^{\text{CBO}})$. In panel (c), the hopping is modified by a pure imaginary number to account for the chiral flux $-(t \pm i\lambda^{\text{CFP}})$, where the sign is indicated by the directions of the arrows. Panel (d): A schematic depiction of a two-terminal device to study quantum transport behavior of the topological superconducting phase discovered in this work, where an $(L \times W)$ -sized central scattering region is constructed by translating the inset minimal unit along the red and green vectors L and W times, respectively, with the atoms (with dangling bonds) on both edges trimmed.

and $\hat{\mathbf{d}}_{ij}$ is the unit vector along the hopping direction from the site j to the site i , and $\mathbf{s} = (s_1, s_2, s_3)$ is the spin Pauli matrix vector. The last term H_{SC} accounts for the spin-singlet s wave and $d_{x^2-y^2}$ wave superconductivity with pairing potential, respectively, the isotropic Δ^s and the anisotropic $\Delta_{ij}^{d_{x^2-y^2}} = \Delta^{d_{x^2-y^2}} \cos(2\phi_{ij})$ [49–53], where ϕ_{ij} is the azimuthal angle of $\hat{\mathbf{d}}_{ij}$, and more details on model construction can be found in Sec. SI of the Supplemental Materials (SM) [54].

Topological superconducting phases.—The model Eq. (1) provides us the opportunity to study the quantum phases from the combination of the three CDW orderings and the two superconducting pairings. As shown by the dashed red bands in panels (a)–(f) of Fig. 2, when the system is free of RSOC ($\alpha = 0.0$), with a proper set of parameters, insulating states can be obtained across all the situations under consideration. And the two superconducting pairings do not render the band structures with much

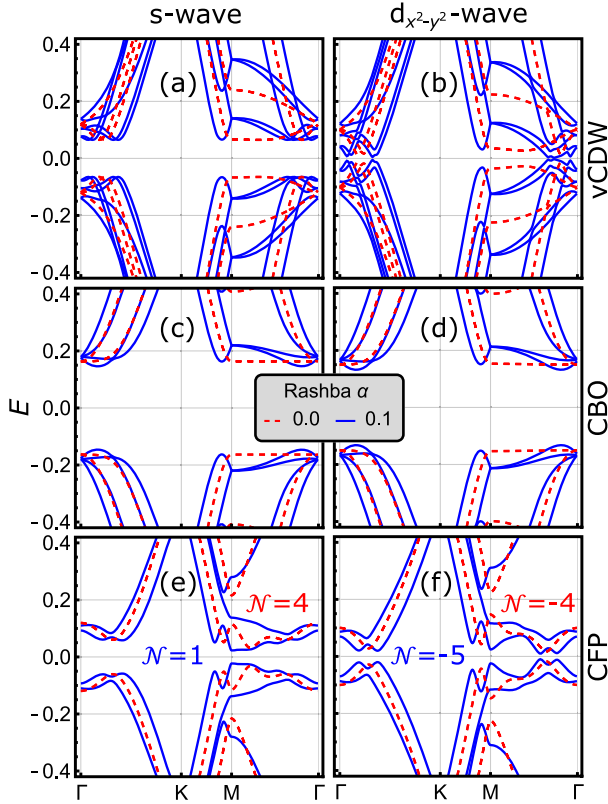


FIG. 2. Bulk band structures by combination of three CDW phases and two superconducting pairings. Panels (a)–(d): Without breaking the time-reversal symmetry, a phase with a non-vanishing BdG Chern number cannot be found from the first two CDW phases. Panels (e),(f): Topologically nontrivial superconducting phases emerge from the last CDW order. Other parameters are $\mu = 0.1$, $\lambda^{\text{vCDW/CBO/CFP}} = 0.25$, $\Delta^s = 0.065$, and $\Delta^{d_{x^2-y^2}} = 0.15$. All energy dimensional quantities are measured in t .

difference for each CDW state. Because the first two CDW (vCDW and CBO) states respect time-reversal symmetry, a nonzero BdG Chern number is not expectable. On the contrary, as the pure CFP carries a nonvanishing Chern number $\mathcal{C} = 2$ (with spin degeneracy), a corresponding BdG model in the same phase reasonably doubles that value. The RSOC ($\alpha = 0.1$) lifts degeneracy at most of the lattice momentum points. Although it makes the band structures more complicated, for vCDW and CBO states, a nontrivial phase is still missing. However, the RSOC induces topological phase transitions for the CFP order, and odd integer BdG Chern numbers can be acquired $\mathcal{N} = 1$ for s -wave and $\mathcal{N} = -5$ for $d_{x^2-y^2}$ -wave pairing, respectively.

A more thorough perspective can be obtained by investigating the topological phase diagram in the Δ - μ space, with color encoding the logarithm of band gap. We first check the case of s wave in Fig. 3. When RSOC does not exist ($\alpha = 0.0$), the BdG model in Eq. (1) just simply doubles the CFP ($\mathcal{N} = 4 = 2\mathcal{C}$) in most area of the phase

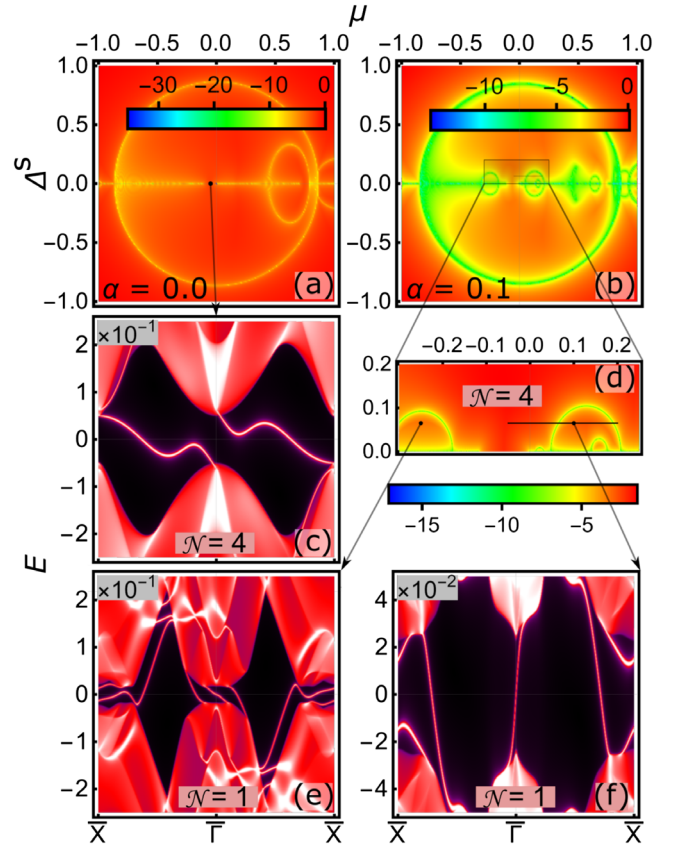


FIG. 3. Phase diagrams for CFP with s -wave superconducting pairings and relevant gapless edge states for TSC. Panel (a): Without RSOC, most region occupied by the $\mathcal{N} = 4$ phase, whose corresponding edge states are shown in panel (c), with spin degeneracy. Panel (b): With RSOC, TSC phases appear, where the region of interest is enlarged in panel (d), and the edge states of two typical TSC phases are respectively shown in panels (e) and (f). The horizontal line segment in panel (d) indicates the parameter samplings for transport study part of this work shown in Fig. 4.

space [see Fig. 3(a)] and its corresponding spectral function data is presented in Fig. 3(c), where the gapless edge state chirality concurs with the BdG Chern number, with the spin degeneracy understood. There is a major yellow phase boundary (seemly a circle), beyond which it is a totally trivial phase. And the size of that phase border is directly related to the value of λ_{CFP} . When a finite RSOC plays its role ($\alpha = 0.1$), some new regions with various shapes and corresponding boundaries appear accordingly from the vanishing-Rashba framework [see Fig. 3(b) and its relevant part enlarged in Fig. 3(d)]. At least two adiabatically unconnected TSC phases both with $\mathcal{N} = 1$ are among them, whose corresponding scenarios of gapless modes are displayed, respectively, in the panels (e) and (f) of Fig. 3. One can see that, although possessing the same Chern number, the situations of gapless modes of the two phases are very different from each other. This CFP-based TSC phase diagram possesses more complexity than its

square-lattice counterpart [10]. The situations for the case of $d_{x^2-y^2}$ wave bear many similarities, where TSC phases appear with the first three negative odd BdG Chern numbers, more on which can be found in the Sec. SIV of the SM [54]. All of the TSC phases shown here have the same characteristics that the total number of edge states is larger than the corresponding Chern number, but none of the net chirality is violated. Besides, we also study the influence of stacking on TSC phases in the third dimension, such as the c direction perpendicular to the kagome plane, which depends on the strength of interlayer coupling. As shown in Fig. S2 of the SM [54], the three-dimensional system would stay in the original chiral TSC phases for a weak interlayer coupling, while exotic topological nodal-point superconductivity can be found when the interlayer coupling is strong. This nodal TSC exhibits Weyl nodes in the bulk and the coexisting flat-band and dispersive Majorana states on the surface. In experiments, the bulk and surface properties of the nodal TSC can be investigated through the thermal Hall transport and angle-resolved photoemission measurements [54].

Transport properties of the gapless edge states.—Now that those TSC phases whose gapless edge modes possess mixed chiralities have been figured out, more can be elucidated by studying their quantum transport behaviors. To start with, we focus on the s -wave case with $\mathcal{N} = 1$, and choose the area where the values of parameters are not very large, where we indicate a straight line path [see Fig. 3(d)] with a fixed pairing potential but a varying chemical potential that walks through the topologically trivial and nontrivial superconducting states. Also in view of the fact that a junction with Chern insulator leads and its derivatives has been shown to have a close relationship with Majorana braiding operations [19], and metal leads are the most experimentally accessible, we build up corresponding two-terminal devices containing a finite sheet with sufficient sizes as its central scattering region, as schematized in Fig. 1(d). The Chern insulator leads are in the state shown in Fig. 3(c) and the metallic leads are those with merely the t term in Fig. (1) and all other parameters are set to be zero. We then find out the coefficients during the processes of the normal electron tunneling (NET), the crossed Andreev reflection (CAR), and the local Andreev reflection (LAR) through the lattice Green's function method with Landauer-Büttiker formalism, with the adaptive partition of the central scattering region used. More on transport study can be found in the Sec. SVI of the SM [54]. The major results are presented in Fig. 4 for a central scattering region with a size of $L \times W$, where the width along the y direction is fixed at a sufficiently large value as $W = 80$, so that the chiral edge states on the upper and the lower edges hardly mix, and the length along the x direction is chosen as $L = 40, 50, \text{ and } 60$. The two leads each have an appropriate semi-infinite lattice translational symmetry along the x direction [67].

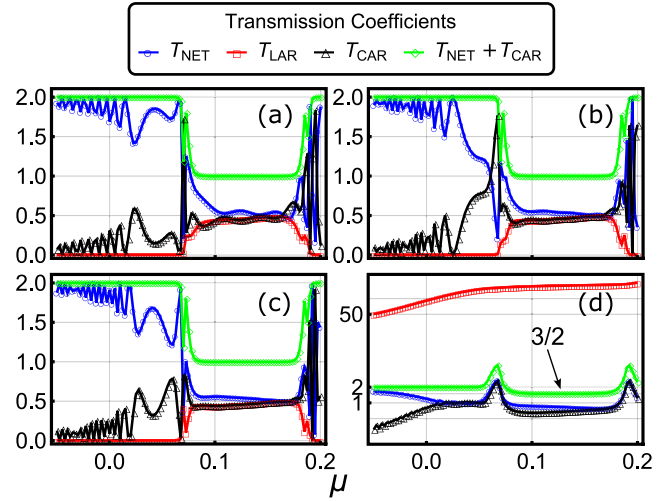


FIG. 4. TSC-related transport coefficients for a two-terminal device with an $(L \times W)$ -sized sheet as its central scattering region. For all panels, the sheet width is fixed at $W = 80$, the superconducting pairing potential is $\Delta^s = 0.065$, and $E = 0^+$. Panels (a)–(c): Chern insulator leads with the sheet length $L = 40, 50, \text{ and } 60$, respectively. Panel (d): Metallic leads with the length $L = 60$. Though the curves behave in a more complex manner, tunneling plateau signals (1 and $\frac{3}{2}$) are still accessible, despite the size of sheet or the category of leads. μ in unit of t .

With the superconducting pairing potential fixed at $\Delta^s = 0.065$ and $E = 0^+$, each coefficient varies with respect to the change of the chemical potential $\mu \in [-0.05, 0.20]$, corresponding to the selected path shown in the phase diagram in Fig. 3(d), where one can see that around $\mu_c \approx 0.07$ there is a topological phase transition. Therefore when the chemical potential is small and the central scattering region is in $\mathcal{N} = 4$ phase, none of the coefficients exceed 2 [Figs. 4(a)–4(c)] because there are only two injecting electron chiral edge states when the leads are all in a quantum anomalous Hall state with $\mathcal{C} = 2$. Specifically, the process of LAR is totally suppressed, and that for NET oscillates under the value of 2, so does the other tunneling process of CAR, so that even though each one of them individually vibrates but together contribute to a plateau signal of 2.

When the chemical potential continues increasing to pass over the critical value ($\mu_c \approx 0.07$), a topological phase transition occurs and now the finite flake enters the TSC phase with $\mathcal{N} = 1$. Then one can see that the amplitudes of coefficients of the both tunneling processes (the NET and the CAR) are reduced, however the LAR coefficient obtains its finite values and largely the same pace with that of the CAR. This coincidence behavior between the two kinds of transport processes has been reported previously [68], but now neither of them is constant with respect to the chemical potential. On the other hand, the tunneling processes together still provide plateau information at a unit value, which can be understood, as the two incoming electron

chiral edge states invoke the two Majorana chiral edge states with the same moving direction in the central scattering region, so that the plateau value drops a half in magnitude after the topological phase transition happens, which moreover is insensitive to the length of the finite sheet [Figs. 4(a)–4(c)]. Finally, when the chemical potential gets close to 0.2, the tunneling plateau rises up to 2 again, and simultaneously the LAR is vanishing, because the system crosses the phase border the second time. We notice that in the course of phase transition (within two small windows of μ around 0.07 and 0.18), the tunneling coefficients experience drastic oscillations. What happens there is yet to be studied but beyond the scope of present work.

With other conditions maintained, now we change the leads to a normal metallic state so that the incoming states not only increase in number but also include bulk wave functions, and the corresponding transport behavior is shown in Fig. 4(d). One can see that in this case, a large number of inscattering electrons are responded by the process for reflection of holes. And the tunneling processes provide a plateau of 2, same as the case with Chern insulating leads [Figs. 4(a)–4(c)] when $\mathcal{N} = 4$, and there is an obvious window of chemical potential where the NET and the CAR approximately have the same coefficient value. When $\mathcal{N} = 1$, however, the plateau changes its previous unit value to 1 with an extra half. This is also comprehensible because now the Majorana chiral edge state with the opposite chirality but localized at the opposite edge is also invoked, so there are totally three Majorana chiral edge states participating in the transport processes.

Furthermore, we study the transport of the chiral TSCs in the presence of disorder and find that they are quite robust against the Anderson-type disorder with a strength well larger than the bulk gap. However, sufficiently strong disorder will destroy the TSC states. More details about the disorder are concluded in Sec. SVII of the SM [54].

Summary and discussion.—To summarize, we establish the connection between topological superconductivity and time-reversal asymmetric CFP state and then confirm a series of chiral TSC phases in the CDW-ordered kagome systems. However, unlike the conventional cases, those new phases are found that edge states highly possibly carry mixed chiralities, e.g., a unit BdG Chern number can support three chiral edge states, yet without violating the chirality constraint. So those phases are expected to provide multiple transport channels and more complexity possibly would be introduced, which is verified in the result of transport coefficients for a two-terminal device. Taken as an example, for the s -wave case with $\mathcal{N} = 1$, when Chern insulator is used as the leads, the tunneling processes together lead to a unity plateau, and the same kind of plateau becomes $\frac{3}{2}$ when there are an abundant of incoming metallic states. Our work reveals the basic transport properties of topological superconductivity when its

gapless edge states carry mixed chiralities, which is different from both the pure chiral and the helical topological superconductors. Moreover, the transport of chiral TSCs exhibits strong robustness with respect to disorder [54]. Because the s wave and the $d_{x^2-y^2}$ wave correspond to different chiral TSC phases, these findings not only provide a clue to distinguish between the superconductivity pairing symmetries but also offer a promising avenue for exploring novel quantum phenomena in the kagome materials AV_3Sb_5 .

This work was supported by the National Natural Science Foundation of China (NSFC, Grants No. 12247181, No. 12222402, No. 12074108, No. 11974062, No. 12147102, and No. 92365101) and the Natural Science Foundation of Chongqing (Grants No. CSTB2022NSCQ-MSX0568 and No. CSTB2023NSCQ-JQX0024), and the Fundamental Research Funds for the Central Universities (Grant No. 2023CDJXY-048). Simulations were performed on Hefei advanced computing center.

*donghuixu@cqu.edu.cn

†rcwang@cqu.edu.cn

- [1] H. K. Onnes, *Proceedings* **13**, 1274 (1911).
- [2] J. Bardeen, L. N. Cooper, and J. R. Schrieffer, *Phys. Rev.* **106**, 162 (1957).
- [3] K. v. Klitzing, G. Dorda, and M. Pepper, *Phys. Rev. Lett.* **45**, 494 (1980).
- [4] D. J. Thouless, M. Kohmoto, M. P. Nightingale, and M. den Nijs, *Phys. Rev. Lett.* **49**, 405 (1982).
- [5] Y. Hatsugai, *Phys. Rev. Lett.* **71**, 3697 (1993).
- [6] F. D. M. Haldane, *Phys. Rev. Lett.* **61**, 2015 (1988).
- [7] C.-Z. Chang *et al.*, *Science* **340**, 167 (2013).
- [8] C.-Z. Chang, C.-X. Liu, and A. H. MacDonald, *Rev. Mod. Phys.* **95**, 011002 (2023).
- [9] M. Nakahara, *Geometry, Topology and Physics*, 2nd ed. (CRC Press, Taylor & Francis Ltd, Boca Raton, Florida, 2003).
- [10] X.-L. Qi, T. L. Hughes, and S.-C. Zhang, *Phys. Rev. B* **82**, 184516 (2010).
- [11] N. Read and D. Green, *Phys. Rev. B* **61**, 10267 (2000).
- [12] X.-L. Qi and S.-C. Zhang, *Rev. Mod. Phys.* **83**, 1057 (2011).
- [13] J. Alicea, *Rep. Prog. Phys.* **75**, 076501 (2012).
- [14] C. Beenakker, *Annu. Rev. Condens. Matter Phys.* **4**, 113 (2013).
- [15] S. R. Elliott and M. Franz, *Rev. Mod. Phys.* **87**, 137 (2015).
- [16] F. Wilczek, *Nat. Phys.* **5**, 614 (2009).
- [17] C. Nayak, S. H. Simon, A. Stern, M. Freedman, and S. Das Sarma, *Rev. Mod. Phys.* **80**, 1083 (2008).
- [18] T. Karzig, C. Knapp, R. M. Lutchyn, P. Bonderson, M. B. Hastings, C. Nayak, J. Alicea, K. Flensberg, S. Plugge, Y. Oreg, C. M. Marcus, and M. H. Freedman, *Phys. Rev. B* **95**, 235305 (2017).
- [19] B. Lian, X.-Q. Sun, A. Vaezi, X.-L. Qi, and S.-C. Zhang, *Proc. Natl. Acad. Sci. U.S.A.* **115**, 10938 (2018).
- [20] Y.-F. Zhou, Z. Hou, and Q.-F. Sun, *Phys. Rev. B* **99**, 195137 (2019).

- [21] S. Nadj-Perge, I. K. Drozdov, B. A. Bernevig, and A. Yazdani, *Phys. Rev. B* **88**, 020407(R) (2013).
- [22] B. Braunecker and P. Simon, *Phys. Rev. Lett.* **111**, 147202 (2013).
- [23] B. R. Ortiz, S. M. L. Teicher, Y. Hu, J. L. Zuo, P. M. Sarte, E. C. Schueller, A. M. Abeykoon, M. J. Krogstad, S. Rosenkranz, R. Osborn, R. Seshadri, L. Balents, J. He, and S. D. Wilson, *Phys. Rev. Lett.* **125**, 247002 (2020).
- [24] X. Feng, K. Jiang, Z. Wang, and J. Hu, *Sci. Bull.* **66**, 1384 (2021).
- [25] X. Feng, Y. Zhang, K. Jiang, and J. Hu, *Phys. Rev. B* **104**, 165136 (2021).
- [26] G. Liu, X. Ma, K. He, Q. Li, H. Tan, Y. Liu, J. Xu, W. Tang, K. Watanabe, T. Taniguchi, L. Gao, Y. Dai, H.-H. Wen, B. Yan, and X. Xi, *Nat. Commun.* **13**, 3461 (2022).
- [27] D. Song, L. Zheng, F. Yu, J. Li, L. Nie, M. Shan, D. Zhao, S. Li, B. Kang, Z. Wu, Y. Zhou, K. Sun, K. Liu, X. Luo, Z. Wang, J. Ying, X. Wan, T. Wu, and X. Chen, *Sci. China Phys. Mech. Astron.* **65**, 247462 (2022).
- [28] Z. Hao *et al.*, *Phys. Rev. B* **106**, L081101 (2022).
- [29] K. Jiang, T. Wu, J.-X. Yin, Z. Wang, M. Z. Hasan, S. D. Wilson, X. Chen, and J. Hu, *Natl. Sci. Rev.* **10**, nwac199 (2023).
- [30] H. Chen, B. Hu, Y. Ye, H. Yang, and H.-J. Gao, *Chin. Phys. B* **31**, 097405 (2022).
- [31] Y. Zhong *et al.*, *Nature (London)* **617**, 488 (2023).
- [32] J.-X. Yin, B. Lian, and M. Z. Hasan, *Nature (London)* **612**, 647 (2022).
- [33] J.-T. Jin, K. Jiang, H. Yao, and Y. Zhou, *Phys. Rev. Lett.* **129**, 167001 (2022).
- [34] S. Zhou and Z. Wang, *Nat. Commun.* **13**, 7288 (2022).
- [35] L. Zheng, Z. Wu, Y. Yang, L. Nie, M. Shan, K. Sun, D. Song, F. Yu, J. Li, D. Zhao, S. Li, B. Kang, Y. Zhou, K. Liu, Z. Xiang, J. Ying, Z. Wang, T. Wu, and X. Chen, *Nature (London)* **611**, 682 (2022).
- [36] F. H. Yu, D. H. Ma, W. Z. Zhuo, S. Q. Liu, X. K. Wen, B. Lei, J. J. Ying, and X. H. Chen, *Nat. Commun.* **12**, 3645 (2021).
- [37] B. R. Ortiz, L. C. Gomes, J. R. Morey, M. Winiarski, M. Bordelon, J. S. Mangum, I. W. H. Oswald, J. A. Rodriguez-Rivera, J. R. Neilson, S. D. Wilson, E. Ertekin, T. M. McQueen, and E. S. Toberer, *Phys. Rev. Mater.* **3**, 094407 (2019).
- [38] Y. Ren, H.-C. Jiang, Z. Qiao, and D. N. Sheng, *Phys. Rev. Lett.* **126**, 117602 (2021).
- [39] S. Peng, Y. Han, G. Pokharel, J. Shen, Z. Li, M. Hashimoto, D. Lu, B. R. Ortiz, Y. Luo, H. Li, M. Guo, B. Wang, S. Cui, Z. Sun, Z. Qiao, S. D. Wilson, and J. He, *Phys. Rev. Lett.* **127**, 266401 (2021).
- [40] F. Yu, X. Zhu, X. Wen, Z. Gui, Z. Li, Y. Han, T. Wu, Z. Wang, Z. Xiang, Z. Qiao, J. Ying, and X. Chen, *Phys. Rev. Lett.* **128**, 077001 (2022).
- [41] Y. Luo *et al.*, *Phys. Rev. B* **105**, L241111 (2022).
- [42] S.-W. Kim, H. Oh, E.-G. Moon, and Y. Kim, *Nat. Commun.* **14**, 591 (2023).
- [43] C. Mu, Q. Yin, Z. Tu, C. Gong, H. Lei, Z. Li, and J. Luo, *Chin. Phys. Lett.* **38**, 077402 (2021).
- [44] H. Luo, Q. Gao, H. Liu, Y. Gu, D. Wu, C. Yi, J. Jia, S. Wu, X. Luo, Y. Xu, L. Zhao, Q. Wang, H. Mao, G. Liu, Z. Zhu, Y. Shi, K. Jiang, J. Hu, Z. Xu, and X. J. Zhou, *Nat. Commun.* **13**, 273 (2022).
- [45] W. Duan, Z. Nie, S. Luo, F. Yu, B. R. Ortiz, L. Yin, H. Su, F. Du, A. Wang, Y. Chen, X. Lu, J. Ying, S. D. Wilson, X. Chen, Y. Song, and H. Yuan, *Sci. China Phys. Mech. Astron.* **64**, 107462 (2021).
- [46] X.-L. Feng, K. Jiang, and J.-P. Hu, *Acta Phys. Sin.* **71**, 118103 (2022).
- [47] Z. Liang, X. Hou, F. Zhang, W. Ma, P. Wu, Z. Zhang, F. Yu, J.-J. Ying, K. Jiang, L. Shan, Z. Wang, and X.-H. Chen, *Phys. Rev. X* **11**, 031026 (2021).
- [48] H.-S. Xu, Y.-J. Yan, R. Yin, W. Xia, S. Fang, Z. Chen, Y. Li, W. Yang, Y. Guo, and D.-L. Feng, *Phys. Rev. Lett.* **127**, 187004 (2021).
- [49] A. M. Black-Schaffer, *Phys. Rev. Lett.* **109**, 197001 (2012).
- [50] A. M. Black-Schaffer and C. Honerkamp, *J. Phys. Condens. Matter* **26**, 423201 (2014).
- [51] X. Wu, T. Schwemmer, T. Mller, A. Consiglio, G. Sangiovanni, D. Di Sante, Y. Iqbal, W. Hanke, A. P. Schnyder, M. M. Denner, M. H. Fischer, T. Neupert, and R. Thomale, *Phys. Rev. Lett.* **127**, 177001 (2021).
- [52] A. D. Fedoseev, *Phys. Rev. B* **105**, 155423 (2022).
- [53] D. Perconte, D. Bercioux, B. Dlubak, P. Seneor, F. S. Bergeret, and J. E. Villegas, *Ann. Phys. (Amsterdam)* **534**, 2100559 (2022).
- [54] See Supplemental Material at <http://link.aps.org/supplemental/10.1103/PhysRevLett.131.086601> for further details on model construction and transport calculation, phase diagram and edge modes for $d_{x^2-y^2}$ -wave case, a primary expansion to three dimensions, and disorder response of the chiral TSC, which include Refs. [55–66].
- [55] F. C. de Lima, R. H. Miwa, and E. S. Morell, *Phys. Rev. B* **100**, 155421 (2019).
- [56] L. Ye, M. Kang, J. Liu, F. von Cube, C. R. Wicker, T. Suzuki, C. Jozwiak, A. Bostwick, E. Rotenberg, D. C. Bell, L. Fu, R. Comin, and J. G. Checkelsky, *Nature (London)* **555**, 638 (2018).
- [57] T. Meng and L. Balents, *Phys. Rev. B* **86**, 054504 (2012).
- [58] Y.-T. Zhang, Z. Hou, X. C. Xie, and Q.-F. Sun, *Phys. Rev. B* **95**, 245433 (2017).
- [59] Z. Qiao and J. Wang, *Nanotechnology* **18**, 435402 (2007).
- [60] L. R. F. Lima, A. Dusko, and C. Lewenkopf, *Phys. Rev. B* **97**, 165405 (2018).
- [61] M. B. de Paz, C. Devescovi, G. Giedke, J. J. Saenz, M. G. Vergniory, B. Bradlyn, D. Bercioux, and A. García-Etxarri, *Adv. Quantum Technol.* **3**, 1900117 (2019).
- [62] T. Fukui, Y. Hatsugai, and H. Suzuki, *J. Phys. Soc. Jpn.* **74**, 1674 (2005).
- [63] R. Yu, X. L. Qi, A. Bernevig, Z. Fang, and X. Dai, *Phys. Rev. B* **84**, 075119 (2011).
- [64] J. Zeng, C. Chen, Y. Ren, Z. Liu, W. Ren, and Z. Qiao, *Phys. Rev. B* **106**, L201407 (2022).
- [65] C. H. Lewenkopf and E. R. Mucciolo, *J. Comput. Electron.* **12**, 203 (2013).
- [66] S. Datta, *Electronic Transport in Mesoscopic Systems* (World Publishing Corporation, Beijing, 2004).
- [67] See Fig. 1(d) and its caption for the exact information for the size.
- [68] Q. Li, Y. Han, K. Zhang, Y.-T. Zhang, J.-J. Liu, and Z. Qiao, *Phys. Rev. B* **102**, 205402 (2020).